Eliminating thermal infrared background noise by imaging with undetected photons

Yue Ma ⬤, Nathan Gemmell, Emma Pearce ⬤, Rupert Oulton, and Chris Phillips ⬤

Blackett Laboratory, Imperial College London, London SW7 2AZ, United Kingdom

Spectroscopy and imaging in the mid-infrared (2.5 μm $\sim \lambda \sim$ 25 μm) is bedeviled by the presence of a strong 300-K thermal background at room temperature that makes infrared (IR) detectors decades noisier than can be readily achieved in the visible. The technique of imaging with undetected photons (IUP) exploits the quantum correlations between entangled photon pairs to transfer image information from one spectral region to another, and here we show that it does so in a way that is immune to the thermal background. This means that IUP can be used to perform high-speed photon-counting measurements across the mid-IR spectrum, using uncooled visible detectors that are many times cheaper, faster, and more sensitive than their IR counterparts.

I. INTRODUCTION

The so-called fingerprint region in the mid-infrared (mid-IR) spectrum (2.5 μm $\sim \lambda \sim$ 25 μm) is where many molecules absorb via bond-specific vibronic transitions. This makes it useful for chemical analysis via vibrational spectroscopy in applications [1] that span biochemical, environmental, pharmaceutical, and healthcare sectors.

Recently, specialist spectroscopic imagers have been developed [2] to diagnose and track cancers via the chemical changes associated with the disease [3,4]. However, measurements in this spectral region take place against a large and fluctuating background of thermal IR radiation that peaks at $\lambda \sim$ 10 μm. The associated photon noise typically limits the achievable detectivity of even the best-cooled detectors: The so-called "background limited infrared photodetector" (BLIP) limit. Moreover, the $1/f$ noise character of its intensity fluctuations makes it challenging to eliminate in room-temperature systems where the IR cameras are inherently slow as well as expensive.

As an example, a cooled 1-mm^2 BLIP detector operating at the $\lambda \sim$ 8 μm wavelength used to detect DNA in Ref. [2] would see $\sim$11.7 μW of IR power in the 1176–1234 cm^{-1} measurement range, corresponding to a photon flux of $\sim 5 \times 10^{14}$ s^{-1}. Technical limitations mean that, in fact, room-temperature detectors are noisier than this by several orders of magnitude.

The technique of "imaging with undetected photons" (IUP) in Ref. [5] uses the quantum correlations between entangled photon pairs to transfer image information from one photon to another with a different wavelength. It has the useful property that it allows an IR image to be registered with a detection system, such as a complementary metal-oxide semiconductor

silicon camera, at shorter wavelengths [6–8]. The effect is being extended into the mid-IR not only for imaging [9] but also for spectroscopy [10–12], as both techniques can make use of the interference effects arising from induced coherence without induced emission [13,14]. IUP is often realized using a nonlinear interferometer, such as we model here. At room temperature, a $\lambda \sim$ 8 μm wavelength detector would see a black-body energy $\sim 3.5 \times 10^{15}$ times the energy seen by one detecting at $\lambda \sim$ 1 μm. IUP therefore promises to extend the capability for high-speed and high-sensitivity photon-counting measurements across the mid-IR for the first time, by sidestepping this large thermal background.

However, to realize this advantage, we must first show that the thermal background does not itself significantly affect the undetected photon-imaging system. This requires showing that thermal states cannot also affect the information in the signal channel by "seeding" the parametric down-conversion (PDC) process in the nonlinear crystals in the interferometer (Fig. 1).

PDC seeded by thermal states has been studied in a single-crystal system [15,16]. Separately, the operation of a nonlinear interferometer restricted to Gaussian states has been analyzed [17], but only with photon detection in both paths. More recently the photon measurement of only one path of a seeded nonlinear interferometer has been considered [18], but only with seeding by coherent states and number states.

Here we investigate the effect of thermal background radiation on a nonlinear interferometer where one path is seeded by a thermal state, while the photon number in the other path is measured. This corresponds to the realistic scenario where the image information is extracted from the short wavelength channel, where the detectors are cheap and/or much more sensitive. We find that the quantity which corresponds to the IUP image information, namely, the visibility of the interference fringes in the interferometer, is not affected by thermal seeding by near-infrared wavelengths ($\sim$1 μm). For much longer wavelengths ($\sim$8 μm), the thermal seeding only starts to impact the IUP image quality at black-body temperatures above $\sim$750 K. In fact, if the whole interferometer system is
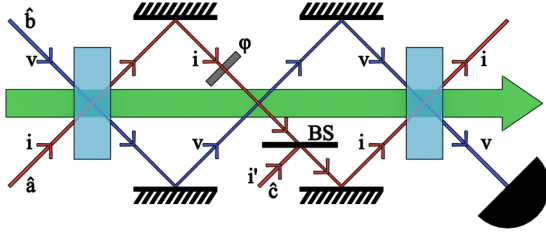
FIG. 1. Schematic of the nonlinear interferometer model. Two nonlinear crystals are pumped by the same continuous-wave laser. Their input modes are treated quantum mechanically. The photon annihilation operator $\hat{b}$ acts on mode v, which has a frequency in the visible range and is unseeded. The other input mode, i, has an IR frequency and is acted on by the photon annihilation operator $\hat{a}$; this mode may be seeded by a thermal state. The addition of the beam splitter (BS) allows us to model the effect of inputting a thermal seed into the second crystal independently. This models the radiation emitted by objects within the interferometer. The two input ports of the beam splitter are the infrared mode i and another mode i′. i′ is also seeded by a thermal state, with a photon annihilation operator $\hat{c}$. A variable phase shifter (ϕ) is included in the IR mode i, to allow us to model the interference fringe visibility.

held at the same temperature, we find that it is completely immune to thermal seeding effects up to extremely high temperatures. This implies that IUP imaging with undetected photons can offer a route to precision IR spectroscopy even in hostile environments where conventional approaches would be impossible.

II. THE MODEL

PDC is an intrinsically pairwise process [15,16], so we need only perform an explicit derivation for the case where each of the two input modes are monochromatic [13,19,20]. In the model (Fig. 1), two nonlinear crystals are pumped by a common continuous-wave laser, frequency ω_p, in the "low-gain" regime (where the pump is not depleted) so the pump is unchanged by the PDC process and is approximated as being classical [20]. The two modes that are seeded into the first crystal and fed by the PDC process are labeled as paths i and v, having frequencies ω_i and ω_v, and corresponding to the IR and visible ranges, respectively. Energy conservation implies that $\omega_i + \omega_v = \omega_p$.

The fringe visibility is modeled by varying the phase of a phase shifter present in the infrared mode between the two crystals. Also included is a variable beam splitter (BS) in the IR mode before it enters the second crystal, which allows us to mix in an independent seeding state through path i′, also at ω_i with the output state of the first crystal.

With the beam splitter set at 100% transmission, the IR input state to the second crystal contains only the IR output state from the first, whereas for a 100% reflection it contains only the additional i′ thermal mode which is independent of the first crystal. This beam splitter acts both as an avenue by which we can model the insertion of thermal radiation and as a means of modeling an object whose transmissivity is to be probed by the system. The photon number in the visible mode is measured at the end of the nonlinear interferometer.

III. EVOLUTION OF THE STATE

We use quantum mechanics to describe the infrared mode i, the visible mode v, and the additional mode i′ for seeding the second crystal. The annihilation (creation) operator in each mode is denoted $\hat{a}$ ($\hat{a}^\dagger$), $\hat{b}$ ($\hat{b}^\dagger$), and $\hat{c}$ ($\hat{c}^\dagger$), respectively. We consider only thermal seeding of the IR modes i and i′. The initial state of the system is, therefore, the tensor product of three density matrices,

$$\rho_0 = \rho_{th,i} \otimes |0\rangle_v \langle 0| \otimes \rho_{th,c}, \tag{1}$$

where $\rho_{th,i}$ is a thermal state for mode i [21,22],

$$\rho_{th,i} = \sum_{n=0}^{\infty} p_n |n\rangle_i \langle n|. \tag{2}$$

Here the probabilities p_n satisfy the Bose-Einstein distribution,

$$p_n = \frac{\exp[-n\hbar\omega_i/k_B T]}{\sum_{m=0}^{\infty} \exp[-m\hbar\omega_i/k_B T]}, \tag{3}$$

where k_B is the Boltzmann constant, T is the temperature, and $|n\rangle$ is a number state. The mean photon number, defined as $n_{th,i} = \text{Tr}(\rho_{th,i}\hat{a}^\dagger\hat{a})$, can be found straightforwardly as

$$n_{th,i} = \frac{1}{\exp[\hbar\omega_i/k_B T] - 1}. \tag{4}$$

The unseeded visible mode v is initially the vacuum state $|0\rangle_v \langle 0|$, and the thermal state $\rho_{th,c}$ denotes the additional mode i′. As is the case in Eqs. (2)–(4), $\rho_{th,c}$ has a mean photon number,

$$n_{th,c} = \frac{1}{\exp[\hbar\omega_i/k_B T'] - 1}. \tag{5}$$

Note that although modes i′ and i have the same frequency, ω_i, the thermal states $\rho_{th,c}$ and $\rho_{th,i}$ correspond to temperatures T' and T, which may differ from each other.

We describe the effect of each optical element in the Schrödinger picture. After passing the first crystal, the state of the system evolves into

$$\rho_1 = \exp[i\xi(\hat{a}\hat{b} + \hat{a}^\dagger\hat{b}^\dagger)]\rho_0 \exp[-i\xi(\hat{a}\hat{b} + \hat{a}^\dagger\hat{b}^\dagger)]. \tag{6}$$

The unitary operator $\exp[i\xi(\hat{a}\hat{b} + \hat{a}^\dagger\hat{b}^\dagger)]$ is the two-mode squeezing operator [23], describing the PDC process involving mode i and mode v, as described by the transformation

$$e^{i\xi(\hat{a}\hat{b}+\hat{a}^\dagger\hat{b}^\dagger)}\hat{a}e^{-i\xi(\hat{a}\hat{b}+\hat{a}^\dagger\hat{b}^\dagger)} = \cosh\xi \cdot \hat{a} - i\sinh\xi \cdot \hat{b}^\dagger, \tag{7}$$

where the parametric gain ξ is assumed to be in the low-gain regime ($\xi \ll 1$) and, without loss of generality, to be real and positive. After the infrared mode i passes through the variable phase shifter, the state of the system becomes

$$\rho_2 = \exp[i\varphi\hat{a}^\dagger\hat{a}]\rho_1 \exp[-i\varphi\hat{a}^\dagger\hat{a}], \tag{8}$$

where φ is the phase shift,

$$e^{-i\varphi\hat{a}^\dagger\hat{a}}\hat{a}^\dagger e^{i\varphi\hat{a}^\dagger\hat{a}} = a^\dagger e^{-i\varphi}. \tag{9}$$

After the beam splitter which mixes the state of mode i with the thermal state of mode i′, the state of the system becomes

$$\rho_3 = \exp[i\kappa(\hat{a}\hat{c}^\dagger + \hat{a}^\dagger\hat{c})]\rho_2 \exp[-i\kappa(\hat{a}\hat{c}^\dagger + \hat{a}^\dagger\hat{c})]. \tag{10}$$

Here the unitary operator $\exp[i\kappa(\hat{a}\hat{c}^\dagger + \hat{a}^\dagger\hat{c})]$ is the beam-splitter operator [23] where the transmissivity is parametrized by the variable $0 \leqslant \kappa \leqslant \pi/2$. The transmissivity and reflectivity of the beam splitter are $\cos^2\kappa$ and $\sin^2\kappa$, respectively [23], as described by the unitary transformation

$$e^{-i\kappa(\hat{a}\hat{c}^\dagger + \hat{a}^\dagger\hat{c})}\hat{a}^\dagger e^{i\kappa(\hat{a}\hat{c}^\dagger + \hat{a}^\dagger\hat{c})} = \cos\kappa \cdot \hat{a}^\dagger - i\sin\kappa \cdot \hat{c}^\dagger. \quad (11)$$

Note that although the quantum states corresponding to the modes i and i' are mixed on the beam splitter, their labels remain unchanged; namely, mode i still corresponds to the path that enters the second crystal. Finally, mode i and mode v pass the second crystal, resulting in the evolved state

$$\rho_4 = \exp[i\xi(\hat{a}\hat{b} + \hat{a}^\dagger\hat{b}^\dagger)]\rho_3 \exp[-i\xi(\hat{a}\hat{b} + \hat{a}^\dagger\hat{b}^\dagger)]. \quad (12)$$

For simplicity, we assume that both crystals have the same gain parameter ξ.

IV. VISIBILITY OF THE INTERFERENCE FRINGES

In practice, the best detectors are available in the visible, so we measure only the mean photon number in mode v, given by $N_v = \text{Tr}(\rho_4 \hat{b}^\dagger \hat{b})$ and calculated to be

$$N_v = (\cosh^2\xi - 1)[(n_{th,i} + 1)\cosh^2\xi(\cos^2\kappa + 1$$
$$+ 2\cos\kappa\cos\varphi) + (n_{th,c} + 1)(1 - \cos^2\kappa)]. \quad (13)$$

The interference fringe visibility is defined as

$$V = \frac{N_{v,max} - N_{v,min}}{N_{v,max} + N_{v,min}}. \quad (14)$$

Note that, although in general, we must find the extremal values of N_v over all possible values of φ, in this case $N_{v,max}$ and $N_{v,min}$ occur at $\varphi = 0$ and π, respectively. Thus, the visibility is

$$V = \frac{2(n_{th,i} + 1)\cosh^2\xi \cdot \cos\kappa}{(n_{th,i}+1)\cosh^2\xi \cdot (1 + \cos^2\kappa) + (n_{th,c} + 1)(1 - \cos^2\kappa)}. \quad (15)$$

Looking at Eq. (15) we note that the fringe visibility will be completely unaffected by the thermal background when the temperature is uniform throughout the interferometer, i.e., when $n_{th,i} = n_{th,c}$; the visibility can only start to deteriorate if the degree of thermal seeding differs between the two crystals. In fact, remarkably, if the outside temperature is the greater, then the thermal background actually improves the fringe visibility.

V. MEAN THERMAL PHOTON NUMBER AND BLACK-BODY RADIATION

Inspecting Eq. (13) one sees that the thermal photons always enter the calculation in the form $(n_{th,i} + 1)$ and $(n_{th,c} + 1)$, where the $+1$ contribution results from the spontaneous nature of the PDC. Setting $n_{th,i} = n_{th,c} = 0$ should reproduce the results of other models that ignore thermal seeding.

Using Eqs. (4) and (5) we find that, at 300 K, $n_{th,i}$ and $n_{th,c}$ evaluate as 1.4×10^{-21} and 2.5×10^{-3} for ω_i values corresponding to wavelengths of 1 and 8 μm, respectively. These are both $\ll 1$ and, therefore, of negligible impact in Eq. (15). We thus conclude that, even if the IUP approach is extended

to wavelengths close to the peak of the 300-K black-body spectrum, the IUP image quality will be essentially immune to the thermal IR background.

At first this result may seem surprising, but it must be remembered that the spectrum of the black-body energy density takes the form [21]

$$\langle W(\omega, T)\rangle d\omega = \langle n(\omega, T)\rangle \cdot \hbar\omega \cdot g(\omega)d\omega. \quad (16)$$

The first term on the right is the photon number [as given by Eq. (4)], the second is the energy per photon, and the third, $g(\omega) = \omega^2/\pi^2 c^3$, is the density of plane-wave photon modes per unit energy, where each has a wave vector $|k| = \omega/c$. The wavelength of the black-body peak, as described by Wien's displacement law, is largely determined by the form of the density of states; at 300 K, it occurs at a wavelength where the mean number of photons per mode is actually quite small.

In our scheme the PDC is an interaction between three photon modes where each interaction involves an IR mode, $\mathbf{k}_i$; a visible one, $\mathbf{k}_v$; and a pump photon, $\mathbf{k}_p$, satisfying the phase-matching condition $\mathbf{k}_p = \mathbf{k}_i + \mathbf{k}_v$ [20]. By its nature, the PDC process occurs even without seeding photons, and we can see that, in all cases of practical interest here (i.e., at 300 K), the effect of thermal seeding is small enough to be ignored. As the argument above applies to each pairwise process involving $\mathbf{k}_i$ and $\mathbf{k}_v$, it applies to the whole process when all the participating modes $\mathbf{k}_i$ are taken into account. In particular, experimental parameters such as the joint spectral density specific to each nonlinear crystal contribute to the weighted sum of different pairwise processes, not the thermal photon number within each process.

We note also that $n_{th} \ll 1$ holds even for optical elements that are usually regarded as strong thermal emitters. For example, a 3000-K incandescent light bulb would only have $n_{th} \sim 10^{-3}$ for 600-nm wavelength modes [22]; i.e., the momentum modes of the radiation field are still mostly empty.

Next we consider higher-temperature environments, to estimate when thermal backgrounds will actually start to degrade the imaging and to determine whether or not it matters which of the two crystals is being seeded.

VI. LONGER WAVELENGTH AND HIGHER TEMPERATURE

As seen in Eq. (4), the values of $n_{th,i}$ and $n_{th,c}$ will clearly increase if either the IR frequency decreases or the ambient temperature increases. For an IR wavelength of 8 μm, $n_{th} \approx 2.5 \times 10^{-3}$ at room temperature $T = 300$ K, but increases to ~ 0.1 by 750 K, at which point one could imagine that the thermal IR background may start to degrade the image. However, even at this level, the attainable image quality using IUP is still likely be many decades better than what one can currently achieve with room-temperature direct IR detectors at this wavelength.

To be specific, in Fig. 2 we show how the mean photon number $n_{th,i}$ (or equivalently $n_{th,c}$) changes as a function of temperature and as a function of the considered wavelength [see Eq. (4)]. For a wavelength of 8 μm, increasing the temperature will increase the mean thermal photon number, and from $T = 750$ K, $n_{th,i}$ starts to reach 0.1 and impact the PDC
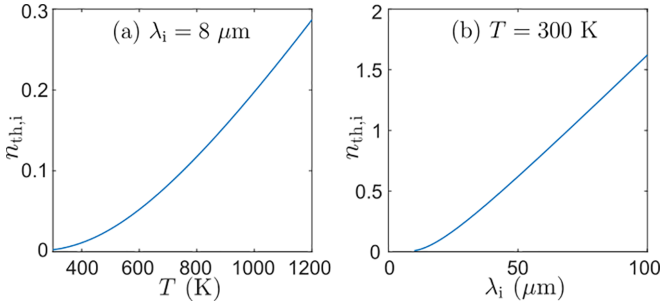
FIG. 2. The mean thermal photon number as a function of (a) temperature, fixing the wavelength as 8 μm. (b) Wavelength, fixing the temperature as 300 K.

process. For a temperature of 300 K, $n_{\text{th,i}}$ only becomes larger than 0.1 for wavelengths larger than 20 μm.

Now we analyze how the visibility in Eq. (15) changes with respect to the parameters κ, $n_{\text{th,c}}$, $n_{\text{th,i}}$, and ξ.

First we examine how the visibility changes with the beam-splitter transmissivity. We define the square root of the transmissivity as $t = \cos \kappa$. It is easy to show that

$$\frac{\partial V}{\partial t} > 0. \quad (17)$$

That is to say that, adding a thermal IR seed field at a point between the two crystals will always reduce the quality of the IUP image. This is because the IR output field from the first crystal has a phase that is linked to that of its visible output in a nonstochastic way. This relative phase information is partially destroyed, and IUP fringe visibility is consequently reduced, when the thermal IR, with its entirely random phase, is added in. When t is reduced to 0, the fringe visibility also vanishes, as the IR entering the second crystal is composed completely of random phase-independent thermal seeding. Both the maximum and the zero values of fringe visibility (corresponding to $t = 1$ and 0, respectively) are independent of other parameters such as $n_{\text{th,i}}$, $n_{\text{th,c}}$, or ξ. In Fig. 3(a), we plot the visibility as a function of $\cos \kappa$, fixing the other parameters as $n_{\text{th,i}} = 0.2$, $n_{\text{th,c}} = 0.15$, and $\xi = 0.03$.

We next study how the visibility changes with the mean photon number of the thermal state to be seeded into the second crystal. Again we find

$$\frac{\partial V}{\partial n_{\text{th,c}}} < 0. \quad (18)$$

With similar reasoning as in the previous paragraph, the more the phase of the beam entering the second crystal is disrupted by the addition of the randomly phased thermal radiation, the worse the effect on the IUP image. In Fig. 3(b), we plot the visibility as a function of $n_{\text{th,c}}$, fixing the other parameters as $n_{\text{th,i}} = 0.2$, $\xi = 0.03$, and $\kappa = 0.05\pi$. Note that even for $n_{\text{th,c}} = 0$, the visibility is less than 1. This is because we have set the beam-splitter transmissivity to be less than unity, thereby mixing the output of the first crystal with the vacuum. Since the vacuum does not have a well-defined phase, mixing it with the output of the first crystal before entering the second crystal also reduces the interference visibility.
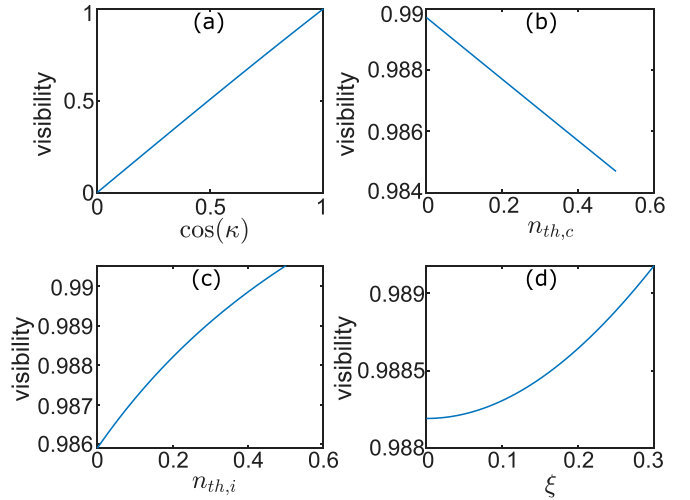

FIG. 3. Visibility of the nonlinear interferometer as a function of (a) the square root of the beam-splitter transmissivity, $\cos \kappa$, where we have chosen $n_{\text{th,i}} = 0.2$, $n_{\text{th,c}} = 0.15$, and $\xi = 0.03$ (b) the mean photon number of the thermal seeding of the second crystal $n_{\text{th,c}}$, where we have chosen $n_{\text{th,i}} = 0.2$, $\xi = 0.03$, and $\kappa = 0.05\pi$; (c) the mean photon number of the thermal seeding of the first crystal $n_{\text{th,i}}$, where we have chosen $n_{\text{th,c}} = 0.15$, $\xi = 0.03$, and $\kappa = 0.05\pi$; and (d) the squeezing parameter of the nonlinear crystals ξ, where we have chosen $n_{\text{th,i}} = 0.2$, $n_{\text{th,c}} = 0.15$, and $\kappa = 0.05\pi$.

Next we consider how the fringe visibility changes with the mean photon number of the thermal state seeding the first crystal. We have

$$\frac{\partial V}{\partial n_{\text{th,i}}} > 0. \quad (19)$$

That is to say that, even though increasing the mean photon number of the thermal state leads to a noisier seed, the visibility increases because this thermal state seeds the entire interferometer. Although the thermal state has a random phase, the relative phase between the down-converted IR and the visible field remains nonstochastic throughout the interferometer. A noisier thermal state also has a larger seeding power and creates more down-converted photon pairs. Despite mixing with the second seeding with a random phase, the overall number of photons carrying nonstochastic phase information is larger, resulting in a larger fringe visibility. In Fig. 3(c), we plot the visibility as a function of $n_{\text{th,i}}$, fixing the other parameters as $n_{\text{th,c}} = 0.15$, $\xi = 0.03$, and $\kappa = 0.05\pi$.

We can also look at how the visibility changes with the parametric gain ξ, which is

$$\frac{\partial V}{\partial \xi} > 0. \quad (20)$$

A larger gain means more photon pairs are generated in the PDC. Similar to the analysis beneath Eq. (19), after the beam splitter, the ratio of the number of coherent photons (whose phase relative to the visible path is well-defined) versus photons with a random phase gets larger, thus increasing the visibility. In Fig. 3(d), we plot the visibility as a function of ξ, fixing the other parameters as $n_{\text{th,i}} = 0.2$, $n_{\text{th,c}} = 0.15$, and $\kappa = 0.05\pi$.

VII. CONCLUSION AND DISCUSSION

We consider a nonlinear interferometer setup where the idler is in the IR frequency range and the signal is in the visible frequency range. A variable phase shifter is present in the idler path, while only the photon number of the signal is measured. We have analytically shown that, if the idler mode is seeded by thermal states before entering both the first and the second crystal, the interference visibility depends on the mean photon number of the seeding thermal states, which is close to 0 for near-infrared and mid-infrared light at room temperature. This implies that the nonlinear interferometer is insensitive to thermal noise from the environment, even when there is a substantial background of IR black-body radiation at the operating wavelength. This is in stark contrast to conventional photon detection schemes where photon noise from the thermal background radiation severely limits the system sensitivity.

We further analyze the regime of longer wavelengths and higher temperatures, showing how the visibility responds differently to a change in the seeding of the first crystal or the second crystal. If the two crystals are subject to the same thermal background in the infrared mode, the seeding does not have an impact on the visibility.

However, the visibility can actually be increased by isolating the second crystal from the thermal background noise that is injected from inside the interferometer, for example, by cooling some of its components. Also the visibility can be improved by injecting thermal radiation at the input mode i, e.g., by shining radiation from a hot object into the interferometer.

[1] R. Salzer and H. W. Siesler, *Infrared and Raman Spectroscopic Imaging* (Wiley & Sons, New York, 2014).

[2] H. Amrania, A. McCrow, and C. Phillips, A benchtop, ultrafast infrared spectroscopic imaging system for biomedical applications, Rev. Sci. Instrum. **80**, 123702 (2009).

[3] H. Amrania, L. Woodley-Barker, K. Goddard, B. Rosales, S. Shousha, G. Thomas, T. McFarlane, M. Sroya, C. Wilhelm-Benartzi, K. Cocks *et al.*, Mid-infrared imaging in breast cancer tissue: An objective measure of grading breast cancer biopsies, Convergent Sci. Phys. Oncol. **4**, 025001 (2018).

[4] H. Amrania, L. Drummond, R. Coombes, S. Shousha, L. Woodley-Barker, K. Weir, W. Hart, I. Carter, and C. Phillips, New IR imaging modalities for cancer detection and for intra-cell chemical mapping with a sub-diffraction mid-IR s-SNOM, Faraday Discuss. **187**, 539 (2016).

[5] G. B. Lemos, V. Borish, G. D. Cole, S. Ramelow, R. Lapkiewicz, and A. Zeilinger, Quantum imaging with undetected photons, Nature (London) **512**, 409 (2014).

[6] A. Búzás, E. K. Wolff, M. G. Benedict, P. Ormos, and A. Dér, Biological microscopy with undetected photons, IEEE Access **8**, 107539 (2020).

[7] A. V. Paterova, S. M. Maniam, H. Yang, G. Grenci, and L. A. Krivitsky, Hyperspectral infrared microscopy with visible light, Sci. Adv. **6**, eabd0460 (2020).

[8] M. Gilaberte Basset, A. Hochrainer, S. Töpfer, F. Riexinger, P. Bickert, J. R. León-Torres, F. Steinlechner, and M. Gräfe, Video-rate imaging with undetected photons, Laser Photonics Rev. **15**, 2000327 (2021).

[9] I. Kviatkovsky, H. M. Chrzanowski, E. G. Avery, H. Bartolomaeus, and S. Ramelow, Microscopy with undetected photons in the mid-infrared, Sci. Adv. **6**, eabd0264 (2020).

[10] C. Lindner, J. Kunz, S. J. Herr, S. Wolf, J. Kießling, and F. Kühnemann, Nonlinear interferometer for Fourier-transform mid-infrared gas spectroscopy using near-infrared detection, Opt. Express **29**, 4035 (2021).

[11] A. V. Paterova, Z. S. D. Toa, H. Yang, and L. A. Krivitsky, Broadband quantum spectroscopy at the fingerprint mid-infrared region, ACS Photonics **9**, 2151 (2022).

[12] Y. Mukai, R. Okamoto, and S. Takeuchi, Quantum Fourier-transform infrared spectroscopy in the fingerprint region, Opt. Express **30**, 22624 (2022).

[13] X. Y. Zou, L. J. Wang, and L. Mandel, Induced Coherence and Indistinguishability in Optical Interference, Phys. Rev. Lett. **67**, 318 (1991).

[14] L. J. Wang, X. Y. Zou, and L. Mandel, Induced coherence without induced emission, Phys. Rev. A **44**, 4614 (1991).

[15] I. P. Degiovanni, M. Bondani, E. Puddu, A. Andreoni, and M. G. Paris, Intensity correlations, entanglement properties, and ghost imaging in multimode thermal-seeded parametric down-conversion: Theory, Phys. Rev. A **76**, 062309 (2007).

[16] I. Degiovanni, M. Genovese, V. Schettini, M. Bondani, A. Andreoni, and M. G. A. Paris, Monitoring the quantum-classical transition in thermally seeded parametric down-conversion by intensity measurements, Phys. Rev. A **79**, 063836 (2009).

[17] C. Sparaciari, S. Olivares, and M. G. A. Paris, Gaussian-state interferometry with passive and active elements, Phys. Rev. A **93**, 023810 (2016).

[18] J. Flórez, E. Pearce, N. R. Gemmell, Y. Ma, G. Bressanini, C. C. Phillips, R. F. Oulton, and A. S. Clark, Enhanced nonlinear interferometry via seeding, arXiv:2209.06749.

[19] U. Leonhardt, Quantum physics of simple optical instruments, Rep. Prog. Phys. **66**, 1207 (2003).

[20] G. Grynberg, A. Aspect, and C. Fabre, *Introduction to Quantum Optics: From the Semi-classical Approach to Quantized Light* (Cambridge University, Cambridge, England, 2010).

[21] R. Loudon, *The Quantum Theory of Light* (Oxford University, Oxford, 2000).

[22] L. Mandel and E. Wolf, *Optical Coherence and Quantum Optics* (Cambridge University, Cambridge, England, 1995).

[23] D. F. Walls and G. J. Milburn, *Quantum Optics* (Springer, Berlin, 2008).